The International Journal of Advanced Manufacturing Technology (2018) 99:1937–1951
https://doi.org/10.1007/s00170-018-2632-3

ORIGINAL ARTICLE

Numerical simulation on an effect of backing plates on joint temperature and weld quality in air and immersed FSW of AA2014-T6

N. D. Ghetiya[1] · K. M. Patel[1]

Received: 7 November 2016 / Accepted: 21 August 2018 / Published online: 29 August 2018

Abstract
In immersed friction stir welding (FSW), the workpiece is fully immersed in the water during welding. Thermal numerical model development of air and immersed FSW is carried out using three-dimensional heat transfer model. FSW joints were produced in AA2014-T6 plate using different backing plates like mild steel, asbestos, and copper in both air and immersed conditions. K-type thermocouples are used to measure the temperature profile at different locations on the workpiece during air and immersed FSW. Commercially available software ANSYS is used to develop thermal numerical model using temperature-dependent material properties of AA2014-T6. The coefficient of friction between a tool and plate has been considered constant throughout the analysis for the simplification for both air and immersed conditions. Simulation results obtained both for air and immersed FSW are in good agreement with those obtained experimentally. It is observed that diffusivity of backing plate affects the temperature of weld region. It is also observed that higher tensile strength and microhardness attained for the joints produced using mild steel backing plate in immersed FSW compared with other backing plates for the same weld parameters.

Keywords Immersed FSW · Tensile strength · Backing plate · Optical microscopy · Temperature

1 Introduction

FSW is a solid state joining process widely used for welding of aluminum alloys. Material does not melt during FSW welding which averts melting-related defects. Welding Institute (TWI, UK) invented FSW process in 1991 [1]. Many high-strength aluminum alloys of 2xxx, 6xxx, and 7xxx series are very difficult to weld because of melting associated defect, can be welded easily using FSW [2–5]. Due to higher strength to weight ratio in the heat treatable aluminum alloys of 2xxx series, find wide spread use in aircraft and aerospace engineering [2, 6]. Mechanical properties of heat treatable aluminum alloys get altered through dissolution of the precipitates during FSW [7]. Recently, many researchers have worked in the area of immersed FSW and obtained remarkable improvement in mechanical properties [8–11]. Fratini et al. [8, 9] accomplished FSW of AA7075-T6 with workpiece immersed in the flowing water. Improvement in the mechanical properties was observed due to reduction in softening in the thermomechanically affected zone (TMAZ) area. Liu et al. [10] compared mechanical properties of AA2219 alloys welded in air and immersed conditions. It was concluded that tensile strength of the immersed joint increased but plasticity was deteriorated. Upadhyay and Reynolds [12] studied the thermal behaviors, torque requirement, and mechanical properties under various thermal boundary conditions in FSW of AA7050-T7. It was concluded that FSW of underwater reduced probe temperature, increased torque and power consumption. Also in underwater joints, decreased in grain size and increased in cooling rate observed compared with air FSW. Same authors investigated the effect of backing plate diffusivity on FSW of AA6056. The result showed that the backing plate conductivity affects the nugget zone (NZ) temperature and tool torque significantly [13]. Authors also studied the effect of ceramic, titanium, steel, and aluminum as backing plate materials on produced temperature and resulted microstructure in FSW of 25.4-mm-thick AA6061 [4]. Murshid et al. [14] reported effect of backing plates in FSW of AA6063-T4 in butt and lap welding using mild steel, stainless steel, and asbestos as backing plate materials. Zhang et al. [15] experimentally investigated the effect of backplate diffusivity on microstructure and mechanical properties of FSW

✉ N. D. Ghetiya
nghetiya@yahoo.com; nilesh.ghetiya@nirmauni.ac.in

[1] Department of Mechanical Engineering, Institute of Technology, Nirma University, Ahmedabad 382481, India

AA2024-T3 joints. Results showed that heat input to the workpiece decreases with increasing backing plate diffusivity. Joint produced with copper backing plate had lowest tensile strength due to defect formed at NZ.

Various author [16–25] used different numerical models based on various assumptions for prediction of thermal history. Frigaard et al. [16] were the first to introduce friction induced model, with constant heat flux from the shoulder and ignoring the heat input from the pin. They developed a process model for FSW for age hardening aluminum alloy. Colegrove et al. [17] developed a three-dimensional CFD model of flow around the threads of the FSW tool. The primary aim was to get better understanding of the material flow around the complex geometry of the FSW tool and also to show the effect of welding speed, rotational speed, and rake angle of the tool on peak temperature. Ulysse [18] reported a three-dimensional finite element (FE)-based coupled thermal and viscoplastic model to simulate metal flow and temperature distribution in FSW process. Chen and Kovacevic [19] used 3D model based on FE analysis to study of the thermal history and thermo-mechanical process during FSW of AA6061-T6. FE simulation software ANSYS was used for the simulation of the FSW process. The heat source incorporated in the model involves the friction between the material and the probe and the shoulder. Gok and Aydin [20] developed finite element model for the FSW process of AZ31 magnesium alloy using the software of DEFORM 3D. Zhang et al. [21] proposed a transient thermal model for FSW, which considered all FSW process including plunging, first dwelling, welding, second dwelling, and cooling. Inverse solution method was used to calculate temperature-dependent friction coefficient to estimate the heat generation rate. Zhang et al. [22] also conducted thermal modeling of underwater FSW with a three-dimensional heat transfer model. The vaporizing characteristics of water were analyzed to fix the boundary conditions in the modeling. FSW experiments were carried out to validate the calculated results.

The past research indicates that the temperature produced during the FSW has a strong influence on the quality of the joint produced. Various numerical models have been developed for the prediction of the thermal history. Different FE software were used for the thermal numerical modeling of FSW process. Looking to the improved weld properties obtained in immersed condition and having very limited knowledge base in this area, it is decided to explore the FSW of AA2014-T6 in immersed condition. It is also evident from the literature that various FSW zone temperature can be changed by changing the backing plate materials having different diffusivity. No attempt has been made in the past to find effect of backing plate materials on the temperature profile observed while FSW in immersed condition. Therefore, an attempt is made as part of this research work to find the effect of various backing plate materials, namely, mild steel, copper, and asbestos on the temperature profile while FSW in both air and immersed conditions experimentally as well as numerically. Also, an attempt is made in this work to establish the effect of backing plate materials on mechanical properties of the immersed FSW joint and same is compared with air FSW.

Table 1 Chemical composition (wt.%) of AA2014-T6 aluminum alloy

Cu	Si	Mg	Mn	Fe	Zn	Ti	Cr	Al
4.64	0.668	0.358	0.58	0.223	0.199	0.020	0.019	93.24

2 Experimental procedure

FSW experiments have been carried out on a vertical milling machine with an indigenously designed fixture to hold the workpiece. The chemical composition and mechanical properties of the workpiece are presented in Tables 1 and 2, respectively. The plates used for welding joint preparation are 300 × 50 × 5 mm in dimension. The tool is made of HSS with 17-mm shoulder diameter and a threaded taper tool pin having 5-mm mean diameter and 4.6-mm height. The threads of 0.9-mm pitch are prepared on the taper pin. A zero tilt angle and penetration depth of 0.3 mm have been applied to welding tool while experimentation. The temperature data for immersed and air FSW is measured using K-type thermocouples and Agilent make data logger. K-type thermocouples of 1.5-mm diameter have been inserted in the mid-thickness on advancing side at a distance of 6, 8, and 11 and 14 mm away from joint line for measuring the temperature distribution during welding process. The layout of the thermocouples placement while FSW of AA2014-T6 plates is shown in Fig. 1.

Experiments have been performed with three backing plates (mild steel, asbestos, and copper) at constant welding 100 mm/min and rotational speed of 1000 rpm in both air and immersed FSW. The temperature profiles obtained for air and immersed FSW using various backing plates are shown in Figs. 2 and 3, respectively. The temperature profiles thus obtained have been used to compare the temperature profiles obtained using simulation.

3 Numerical simulation and results

The limitation of experimentation is that one cannot get temperature at desired location on the plate while FSW. Also, due to

Table 2 Properties of AA2014-T4 aluminum alloy

Tensile strength (MPa)	Density (kg/m^3)	Thermal conductivity (W/m K)	Melting point (°C)	Vickers hardness (HV)	Specific heat (J/kg °C)
470	2800	154	638	150	880

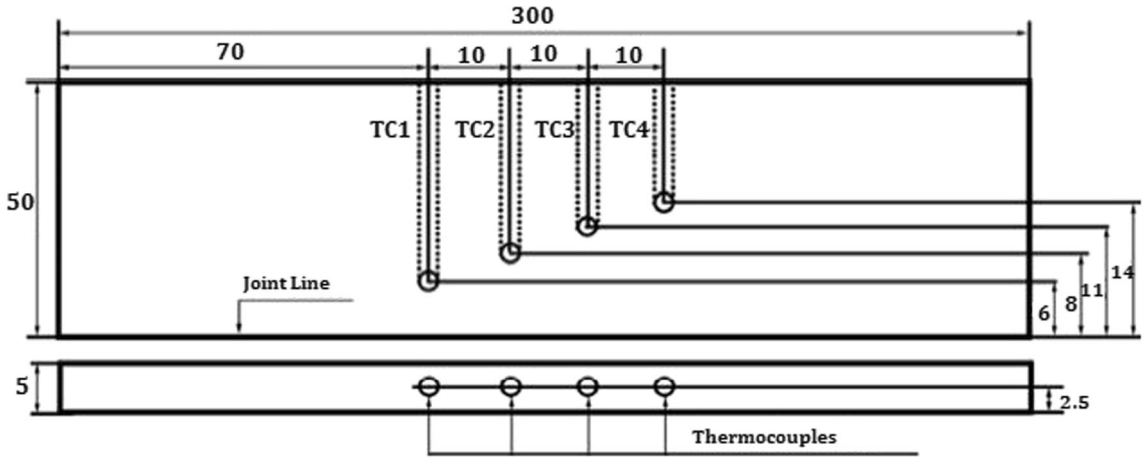

Fig. 1 Thermocouples placement in the weld plate in air and immersed FSW

high cost of experimentation, a numerical model for prediction of temperature during FSW is useful for the analysis. Commercially available FEA software ANSYS is used for development of thermal numerical simulation model. The validation of same has been done with experimentally measured temperature.

3.1 Thermal numerical simulation

The main aim of thermal numerical FE model is to calculate the transient thermal history generated in workpiece during FSW. In the present study, a Poisson's equation for the temperature profile in the plate with the moving heat flux is solved. In the present work, an arbitrary Lagrangian-Eulerian formulation is used to solve the below mentioned equation. The transient temperature T during FSW, which is the function of time t and spatial coordinates (x, y, z), is estimated by the three-dimensional nonlinear heat transfer (Eq. 1) [26].

$$\frac{\partial^2 T}{\partial x^2}+\frac{\partial^2 T}{\partial y^2}+\frac{\partial^2 T}{\partial z^2}+\frac{q(x,y,z,t)}{k}=\frac{1}{\alpha}\frac{\partial T}{\partial t} \tag{1}$$

If the coordinate system is fixed with moving heat source, then mathematical formulation of moving coordinate system will be as follows:

A new coordinate ζ is defined by

$$\zeta = x - ut \tag{2}$$

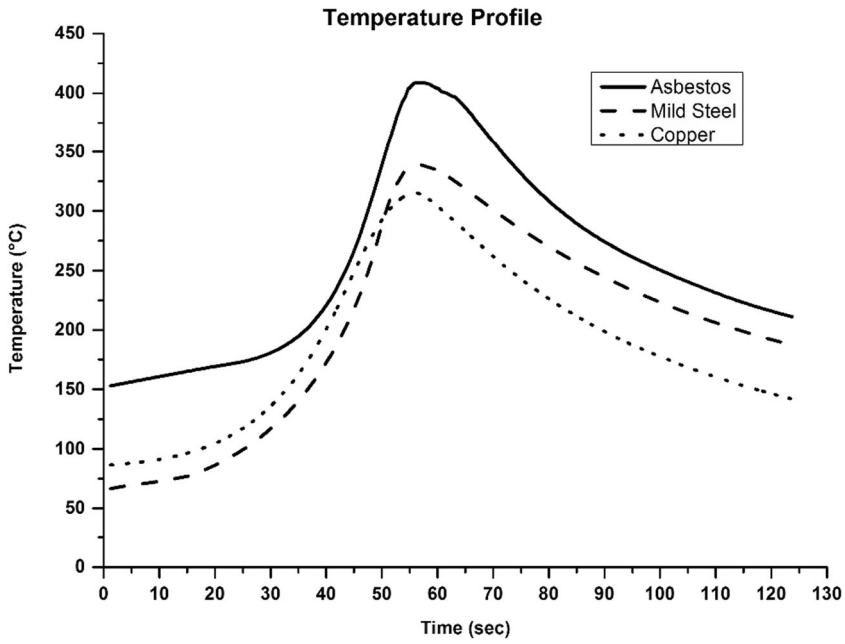

Fig. 2 Variation of temperature with time at 6 mm away from weld line in air FSW

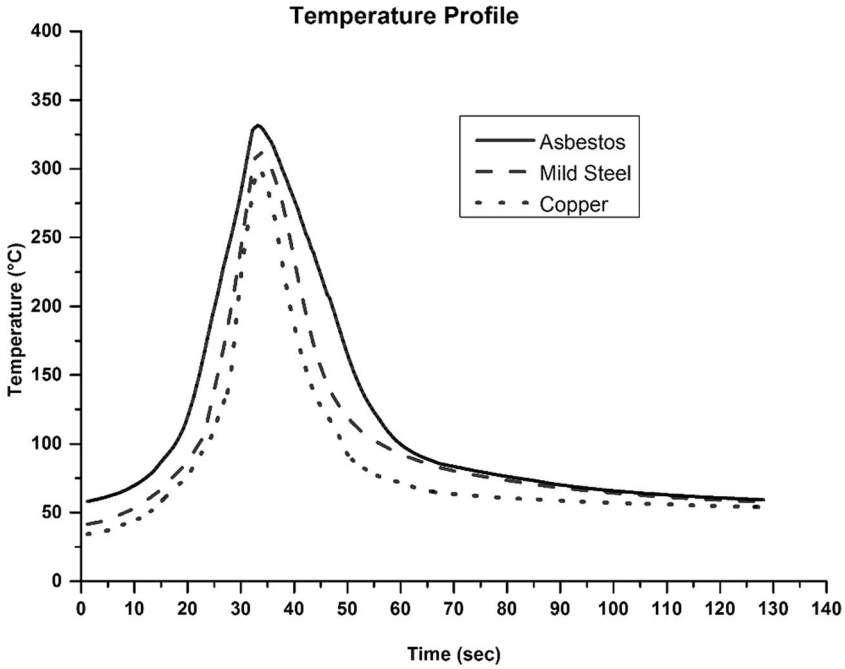

Fig. 3 Variation of temperature with time at 6 mm away from weld line in immersed FSW

With this definition of ζ, the new formulation of governing equation will be as follows:

$$\frac{\partial T(\zeta,y,z,t)}{\partial t} = -u\frac{\partial T}{\partial \zeta} + \frac{\partial T}{\partial t}; \frac{\partial T}{\partial x} = \frac{\partial T}{\partial \zeta} \text{and} \frac{\partial^2 T}{\partial x^2} = \frac{\partial^2 T}{\partial \zeta^2} \quad (3)$$

$$\frac{\partial^2 T}{\partial \zeta^2} + \frac{\partial^2 T}{\partial y^2} + \frac{\partial^2 T}{\partial z^2} + \frac{q(\zeta,y,z,t)}{k} = \frac{1}{\alpha}\frac{\partial T}{\partial t} - \frac{u}{\alpha}\frac{\partial T}{\partial \zeta} \quad (4)$$

Some of the assumptions that are made for the development of thermo-numerical model are as mentioned below:

1. Workpiece material is isotropic and homogenous.
2. No melting occurs during the welding process.
3. Heat transfer from the workpiece to the clamp is negligible.
4. Thermal boundary conditions are symmetrical across the weld centerline.
5. Heat input and convection remain constant throughout the welding process.

The two plates having length 300 mm, width 50 mm, and thickness 5 mm have been considered for numerical model. Symmetric boundary condition has been used on both side of the weld line for reducing simulation time. Workpiece is meshed using a brick element called SOLID70 for the analysis. This element has a three-dimensional thermal conduction capability and can be used for a three-dimensional, steady state, or transient thermal analysis [27]. Element used has eight nodes with single degree of freedom, i.e., temperature at each node. Heat flux or convection is applied as surface load on the faces of element. The main advantage of using this element is that it can easily replace by equivalent structural element for the structural analysis. A SOLID70 and SURF152 elements are used for the transient temperature analysis.

3.2 Material properties

An accurate estimation of temperature is important because the stresses and strain developed in the weld are dependent on the temperature generated. Temperature-dependent thermal properties of AA2014-T6 such as thermal conductivity and specific heat are used for numerical model and same are tabulated in Table 3.

3.3 Boundary conditions used for the simulation

Boundary conditions for FE model are specified as surface load using ANSYS APDL. Radiation heat loss is neglected in the model because the lower surface emissivity by aluminum is

Table 3 Temperature-dependent material properties of AA2014-T6 [28]

Temperature (°C)	Thermal conductivity (W/m K)	Specific heat (J/kg °C)
300	175	880
400	180	900
500	187	950
600	195	980

lower. Convective heat losses to ambient temperature that occurred across all free surfaces of the workpiece are considered for the analysis. Conduction losses that occurred through bottom surface of workpiece to the backing plate are also considered for the analysis. Free natural convection is assumed on the exposed surfaces (the four vertical planes and the top surface), except at the nodes where the shoulder heat input is applied. The contact conductance at the base plate which is in the contact with the fixture is also modeled as equivalent to a convection boundary. Convective heat transfer coefficients for air and water are calculated and have been taken as input on all the surfaces expect bottom surface. To solve the heat conduction equation, a large number of arbitrary constant needs to be determined by specific initial and boundary conditions.

The initial boundary condition in a material for the calculation is given by

$$T(x,y,z,t) = T_0 \tag{5}$$

T_0 is the initial temperature of the workpiece and is assumed to be atmospheric temperature. The energy balance at the workpiece surface leads to few other boundary conditions. Specific heat flows from the shoulder and pin to the workpiece surface while FSW is assumed to be q_s and q_p, respectively. The surfaces other than bottom surface are exposed to the atmosphere, where heat loss takes place due to convection only.

The heat flux boundary condition at the bottom of the workpiece interface is given by

$$-k\frac{\partial T}{\partial n} = q \tag{6}$$

The convective boundary condition for all the surfaces of the workpiece exposed to the air and water is given by

$$-k\frac{\partial T}{\partial n} = h(T-T_0) \tag{7}$$

where n is the normal direction vector of the boundary.

The natural convective coefficient for the air and immersed FSW is calculated using procedure mentioned below. During the early stage of present analysis, the local heat transfer coefficient (h_x) was calculated from the local heat transfer and the local temperature gradient as

$$h_x = \frac{q_{net}}{(T-T_o)} \tag{8}$$

This analysis required a complicated nonlinear solutions resulting in increase in computational time. Later, the overall heat transfer coefficient ($\overline{h}$) is calculated as

$$\overline{h} = \frac{\iint h_x dA.dt}{\iint dA.dt} \tag{9}$$

The overall heat transfer coefficient is also compared with the analytical heat transfer coefficient calculated as [29]

$$h = \frac{Nu \times k}{L} \tag{10}$$

$$Nu = 0.54(R_{al})^{1/4} \tag{11}$$

$$R_{al} = \frac{g\beta(t_s - t_a)L^3 P_r}{\nu^2} \tag{12}$$

$$\beta = \frac{1}{T_f} \tag{13}$$

$$T_f = \frac{(t_s + t_a)}{2} \tag{14}$$

All the properties are evaluated as bulk mean temperature. The analytical values of convective heat transfer coefficient for mild steel, asbestos, and copper as backing plates in air as well as immersed FSW have been calculated using above methodology. The convective heat transfer coefficients for mild steel, asbestos, and copper backing plates in air FSW are 11.14, 11.36, and 10.87 W/m^2 °C, respectively, and in immersed FSW, same are 278.74, 282.61, and 275.80 W/m^2 °C, respectively.

During the study, it is also observed that the overall heat transfer coefficient ($\overline{h}$) was found near to analytical calculated values. Hence, for all further analysis, the overall heat transfer coefficient is assumed constant with value equal to analytical heat transfer coefficient. It should be noted that the assumption of constant heat transfer coefficient leads to great simplification in the analysis with minimum deviation from the actual results. Similar procedure is followed for predicting the overall heat transfer coefficient for the backing plate.

In most of the previous research work involving thermal numerical model development of the air FSW of aluminum alloys, a convective heat transfer coefficients of 10–30 W/m^2 °C has been considered for the surfaces exposed to atmospheric air [23, 30, 31]. In this study, for air FSW, all the surfaces of the workpiece exposed to the air, 11.14, 11.334, and 10.87 W/m^2 °C have been considered as convective heat transfer coefficients for mild steel, asbestos, and copper backing plates, respectively. Whereas for the surfaces completely immersed in water, convective heat transfer coefficients have been considered as 278.74, 282.61, and 275.80 W/m^2 °C for mild steel, asbestos, and copper backing plates, respectively. The heat loss to the backing plate is modeled by assuming the convective coefficient of value 350 W/m^2 °C.

3.4 Heat generation modeling

Heat produced due to friction between the workpiece and the tool shoulder as well as the workpiece and the tool pin has been considered for the modeling. Heat flux from the

shoulder has been calculated considering tool geometry and parameters used for the FSW using Eq. 15 [16]:

$$Q_s = \frac{2}{3}\frac{\pi\mu Pw\left(R_o^3 - R_t^3\right)}{\left(R_o^2 - R_t^2\right)} \tag{15}$$

Heat flux generated by the tool shoulders Q_s can be calculated using Eq. 15, where $N = 1000$ rpm, $F = 2.3$ kN, $v = 100$ mm/min, $R_o = 0.0085$ m, $R_i = 0.002$ m, $\mu = 0.34$, $p = 10{,}133{,}048.28$ Pa, and $\omega = 104.719$ rad/s. The ratio of heat generated by the pin Q_p to shoulder Q_s, 0.128, is considered for the analysis [32]. Transient thermal analysis is used in the present case. The material has been treated as solid. In the numerical modeling, total 47,538 unstructured tetrahedral elements have been selected. Finer mesh size has been used at the edges of plate as well as at the interface of the tool and the plates. An atmospheric temperature was considered as initial temperature of the plate surfaces. Heat generation is calculated based on full slip condition (only friction heat is considered to determine the heat flux distribution at the tool-workpiece interface). Coefficient of friction 0.34 has been fixed by comparing the predicted temperature data with experimentally measured temperature data. In the thermal model, the dwell period of 60 s has been given. As the tool is not modeled separately, plunge in period is not given. A coordinate system has been stimulated after each load step for the analysis. At every load step, a set of elements in the shape of the tool has been selected. The movement of FSW tool is considered for the analysis by creating a circular thin surface of zero thickness on the top surface of workpiece. Total heat flux Q is the summation of Q_p and Q_s and same is applied on the surfaces of the elements. Based on the welding speed of tool, time required to travel a specific distance is calculated and that time is inserted for the first surface of tool in the transient analysis.

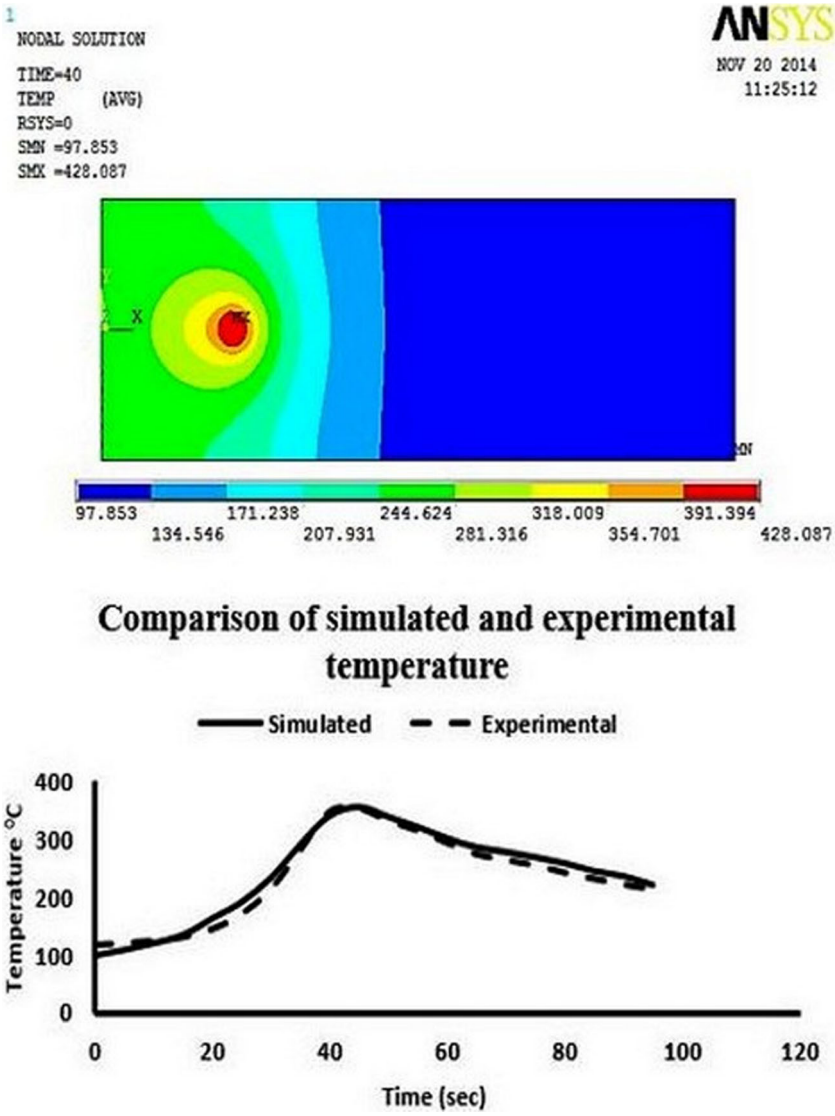

Fig. 4 Simulated results of temperature for mild steel as backing plate in air FSW

For rest of the surfaces, similar procedure is adopted. By doing these, different load steps are created for individual surface of the tool. The conduction (Eq. 5) is solved implicitly using second-order scheme. The conversion criterion for temperature has been selected as 10^{-6}.

3.5 Results and discussion

Transient FE thermal numerical simulation of air and immersed FSW have been carried out using ANSYS. Temperature-dependent material properties of AA 2014-T6 have been used for the simulation. The temperature profile obtained by simulation for air FSW using mild steel backing plate is shown in Fig. 4. Maximum temperature is found below tool shoulder while air FSW using mild steel backing plate. It is found that temperature increases with an increase in the welding time. It is observed that the larger area of the plate has reached high temperature due to lesser convective heat transfer coefficient in air. In the lateral direction or along the width of the plate, temperature is gradually decreasing. The maximum temperature of 350.37 °C has been observed at 6 mm away from the weld line at time $t = 40$ s by the simulation. The experimentally measured temperature at the same location is 339.50 °C. The good agreement between an experimentally measured and the simulated temperature shows that the developed thermal numerical model successfully predicts temperature in NZ within 3.5% of error. Similar trends have been observed in measured and simulated temperature obtained while using asbestos and copper as backing plates in the air FSW. The results of the same are shown in Figs. 5 and 6 Similarly, thermal numerical analysis are carried out for immersed FSW using asbestos, mild steel, and copper backing plates. Figures 7, 8, and 9 show the comparison of simulated and experimental temperature data obtained using

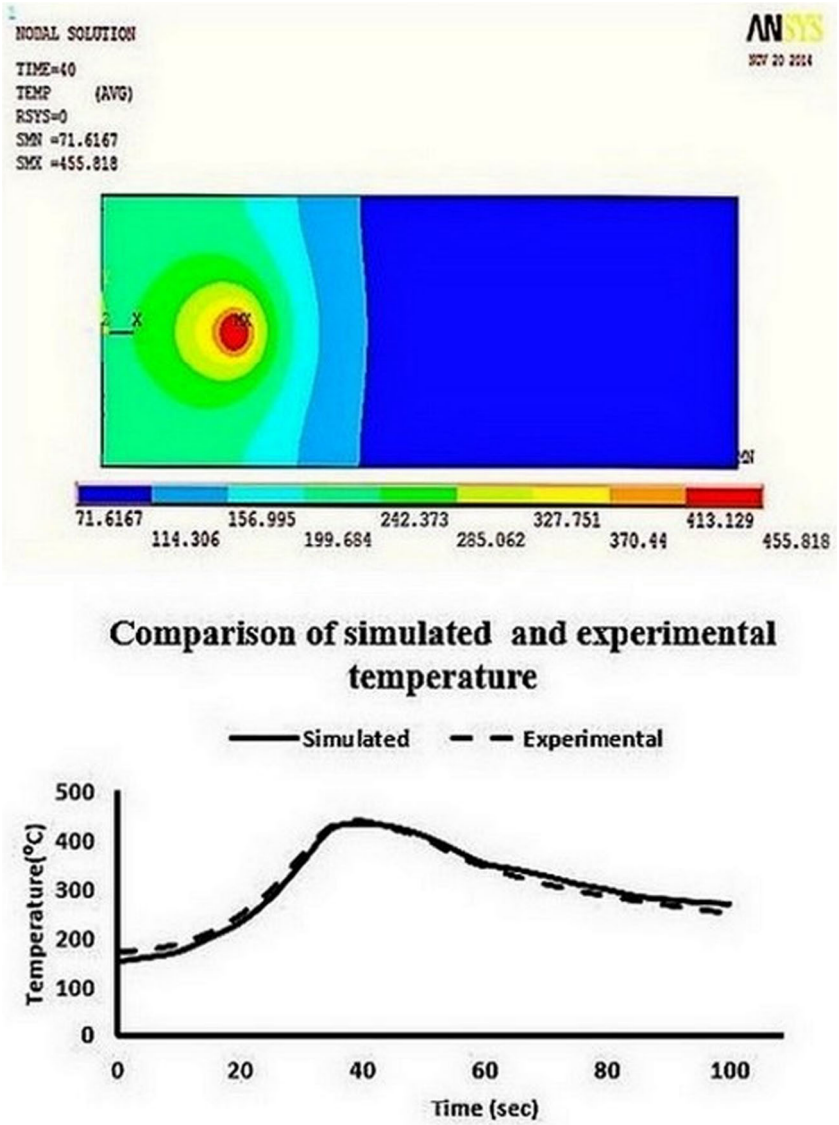

Fig. 5 Simulated results of temperature for asbestos as backing plate in air FSW

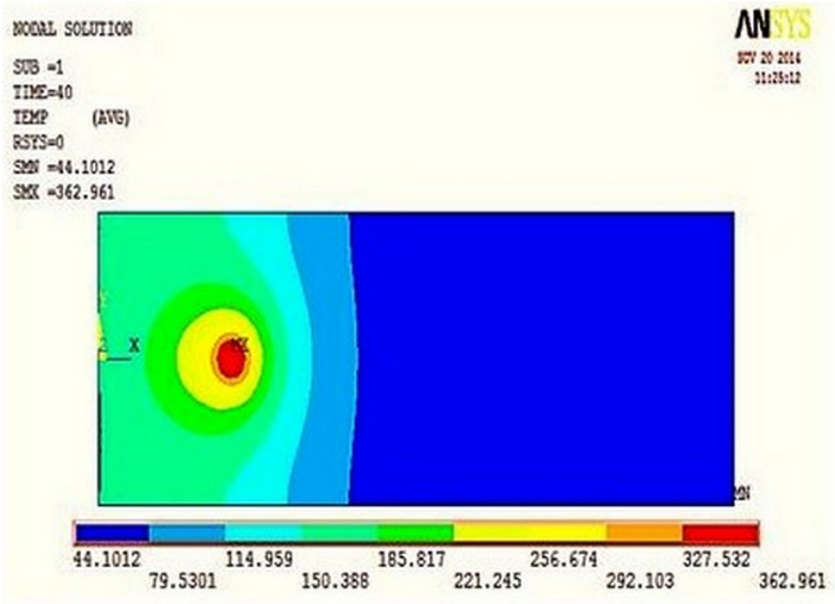

Fig. 6 Simulated results of temperature for copper as backing plate in air FSW

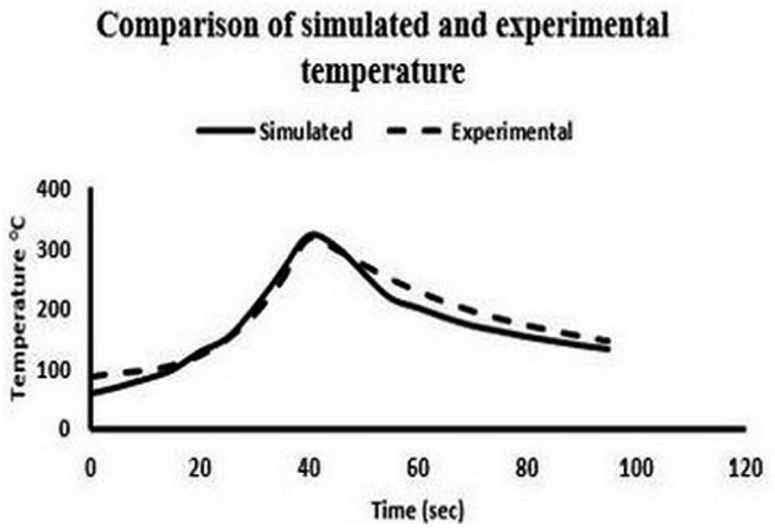

thermocouples. It can be concluded from the graphs that simulated and experimentally measured temperature are in good agreement. The peak temperature obtained using FE simulation differs from the peak temperature obtained experimentally. This may be due to the assumption made for simulation that coefficient of friction is constant throughout welding process, while in real condition, it is found to be dynamic in nature. The inclusion of heat generation due to plastic deformation in the mathematical model may improve the prediction of the temperature profile. For the simplification of the simulation, coefficient of friction 0.34 has been considered constant throughout the analysis for both air and immersed FSW. However, it varies continuously with workpiece temperature while FSW in process. In case of immersed FSW, water boils near the tool also affects the coefficient of friction. Moreover, the heat transfer rate near the tool also differs from the heat transfer rate prevailing in the other parts of the workpieces. This may be another reason for the variation in the temperature distribution obtained experimentally and by simulation.

It can be observed from Figs. 10 and 11 that the difference in the temperature along thickness direction is very small. NZ is found to have more depth and width in the case of air FSW in comparison with immersed FSW due to higher temperature experienced during air FSW. In immersed FSW, peak temperature obtained is lower than that of air FSW and also temperature distribution area having higher temperature is also narrower. The temperature rise and drop with time at the weld line (thermocouple TC1) in air FSW is gradual while in immersed FSW, it is sharp. Temperature rises gradually in air FSW as the tool advances towards the thermocouple because of higher rate of heat transfer in the welding plate. Heat transfer rate in the workpiece is lower in case of immersed FSW

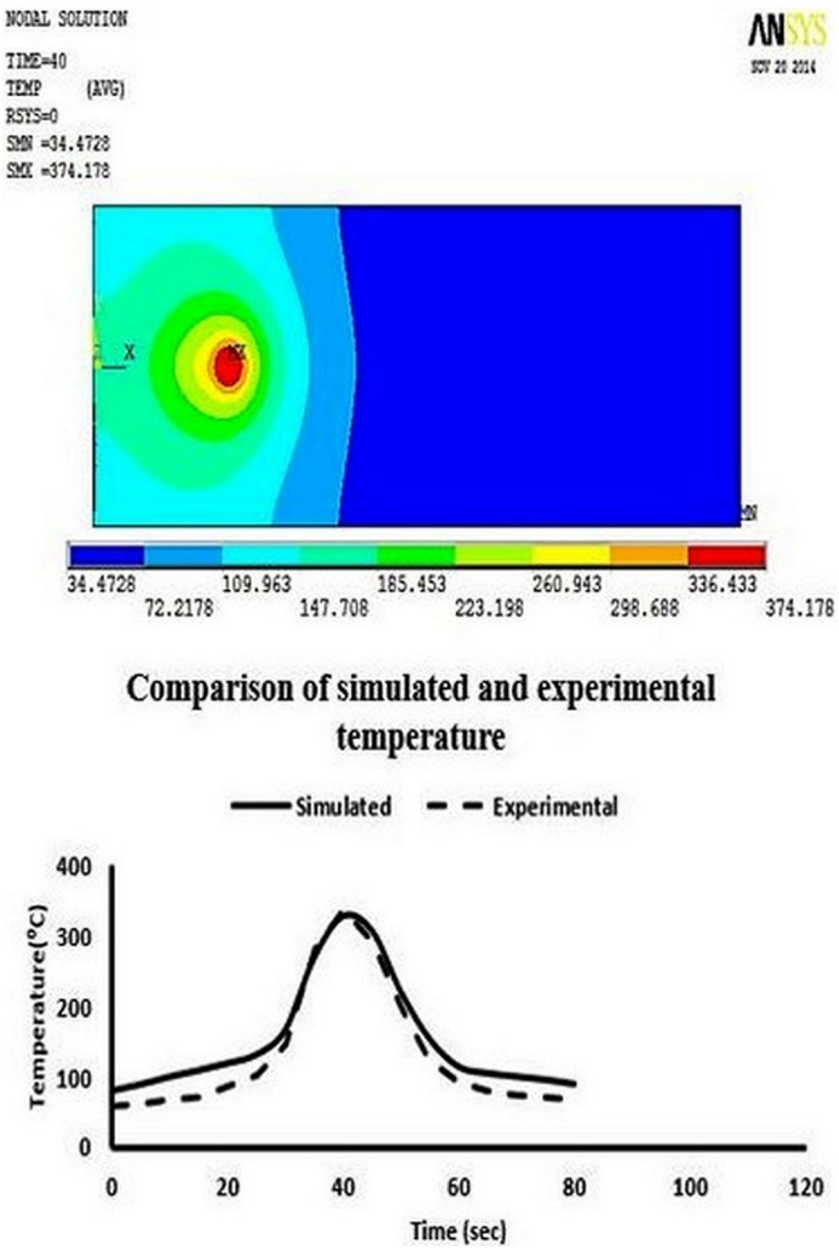

Fig. 7 Simulated results of temperature for asbestos as backing plate in immersed FSW

due to water cooling, and hence, temperature rise is very sharp when tool reaches closed to the thermocouple. Another reason for the sharp rise in temperature in immersed FSW is due to water boiling near the tool.

Decreasing convective heat transfer coefficient of backing plates from copper to asbestos, temperature at NZ is found to increase both in air and immersed FSW. It is also observed that temperature contour changes with the reduction in diffusivity of the backing plates that is an area covered with higher temperature is found to be increased. While comparing temperature profiles obtained for various backing plates, it is found that with an increase in diffusivity of backing plate, sudden increase and decrease in temperature have been observed. This is due to higher heat convection through the workpiece which results into higher cooling. Also, very sharp rise and fall in temperature have been observed in the case of copper backing plate during immersed FSW. It is due to high conductivity of the copper plate and presence of the water above the workpiece. The higher temperature area is very narrow in the case of the copper backing plate compared with other backing plates for both air and immersed FSW.

The quality of the joint obtained while using copper backing plate is inferior in immersed FSW due to insufficient temperature rise in the workpiece which produces the visible defects in the welded workpiece. Even though narrow heat-affected zone is advantageous from the welding point of view, the temperature produced is not sufficient for the good weld. Asbestos backing plate prevents the heat transfer from the

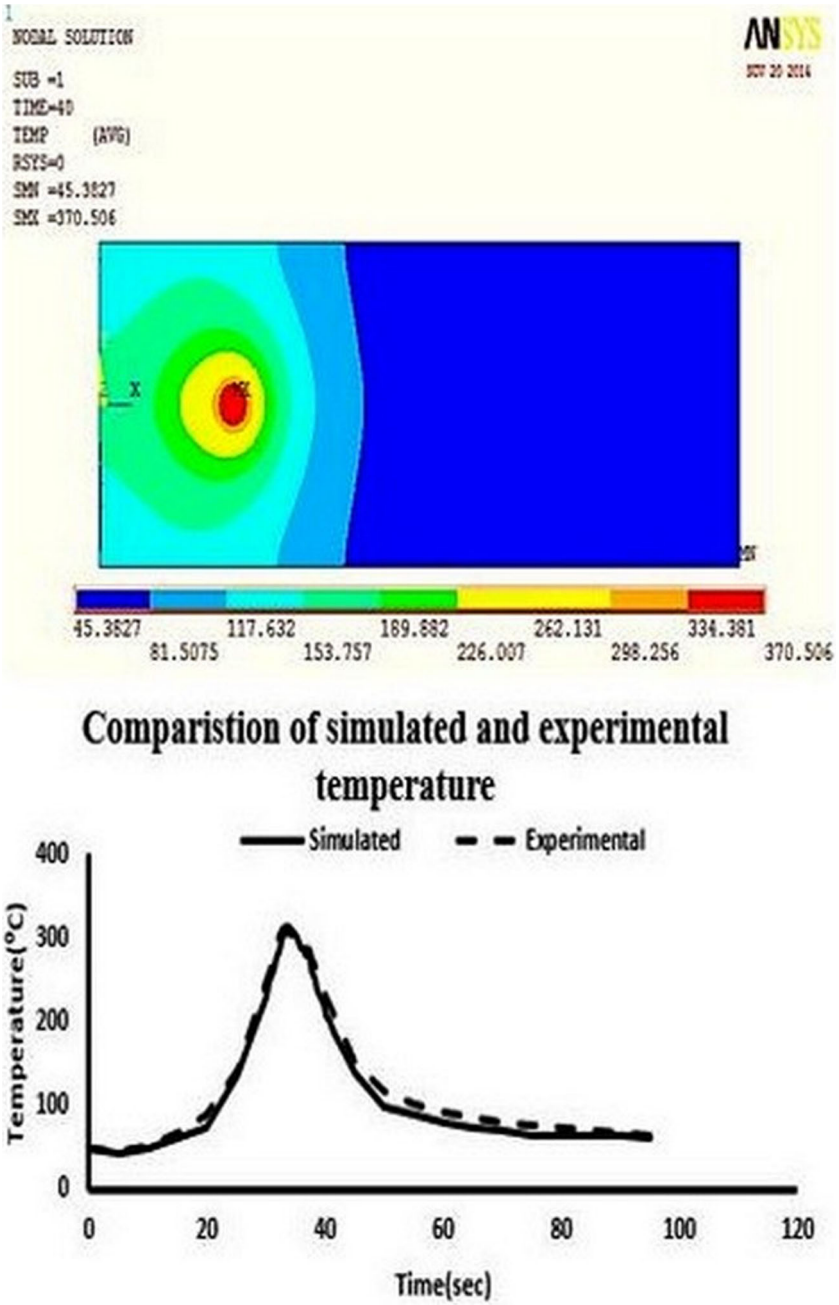

Fig. 8 Simulated results of temperature for mild steel as backing plate in immersed FSW

bottom of the plate. The rise and fall of the temperature is very gradual and time for which material remains at higher temperature is also higher. Due to this, deterioration in the mechanical properties of weld joint is observed. Mild steel backing plate produces the weld without defects due to sufficient heat generation. Also, immersed FSW with mild steel backing plate reduces the dissolution of strengthening precipitates and hence improves the mechanical properties of welded joint.

The tensile strength plots of the FSW joints welded using different welding conditions are shown in Fig. 12. It can be seen that the best tensile strength 332 MPa is obtained for the FSW joint prepared using mild steel backing plate in the immersed FSW which is 20% higher than air FSW. Similarly, lowest tensile strength is obtained for the air FSW joint prepared using asbestos backing plate material. The strength of the joint thus obtained is 50% of the BM tensile strength. It is also observed that immersed FSW joints obtained using the asbestos and mild steel backing plates have higher tensile strength than air FSW joints. In case of a copper backing plate, air FSW joint has higher tensile strength than immersed FSW joint. This is due to high cooling rate obtained using copper backing plate in immersed condition results in the defects at pin region which reduces the tensile strength of the joint.

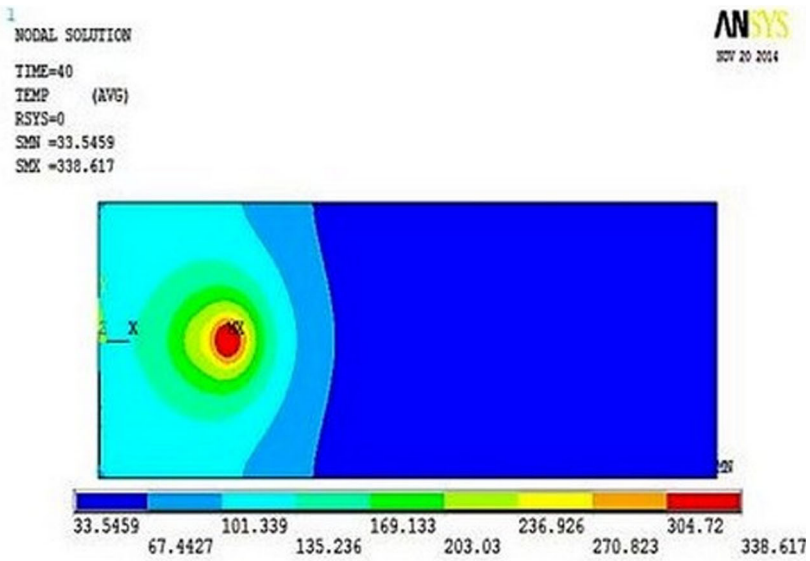

Fig. 9 Simulated results of temperature for copper as backing plate in immersed FSW

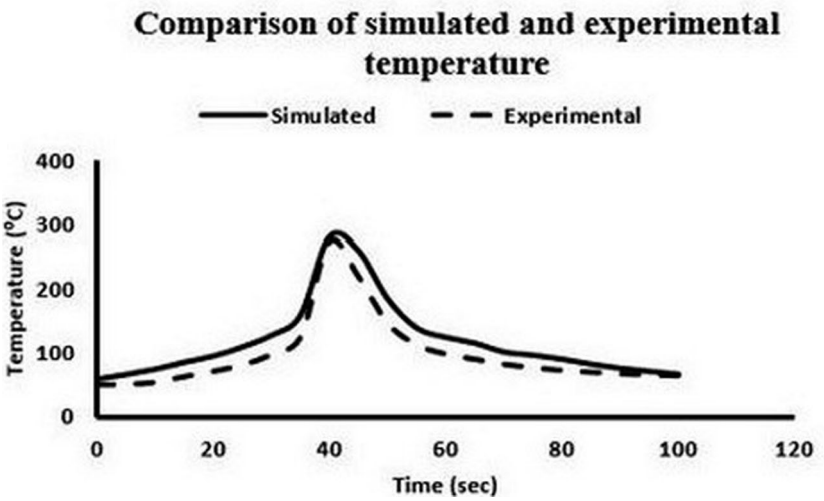

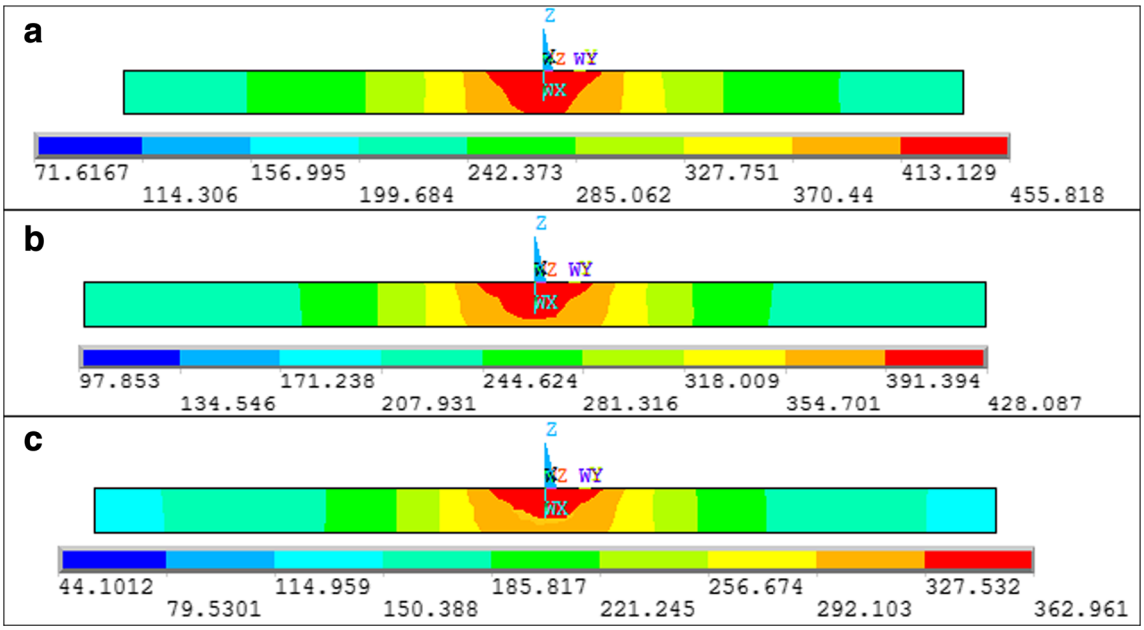

Fig. 10 Temperature distribution for air FSW along thickness direction for **a** asbestos, **b** mild steel, and **c** copper

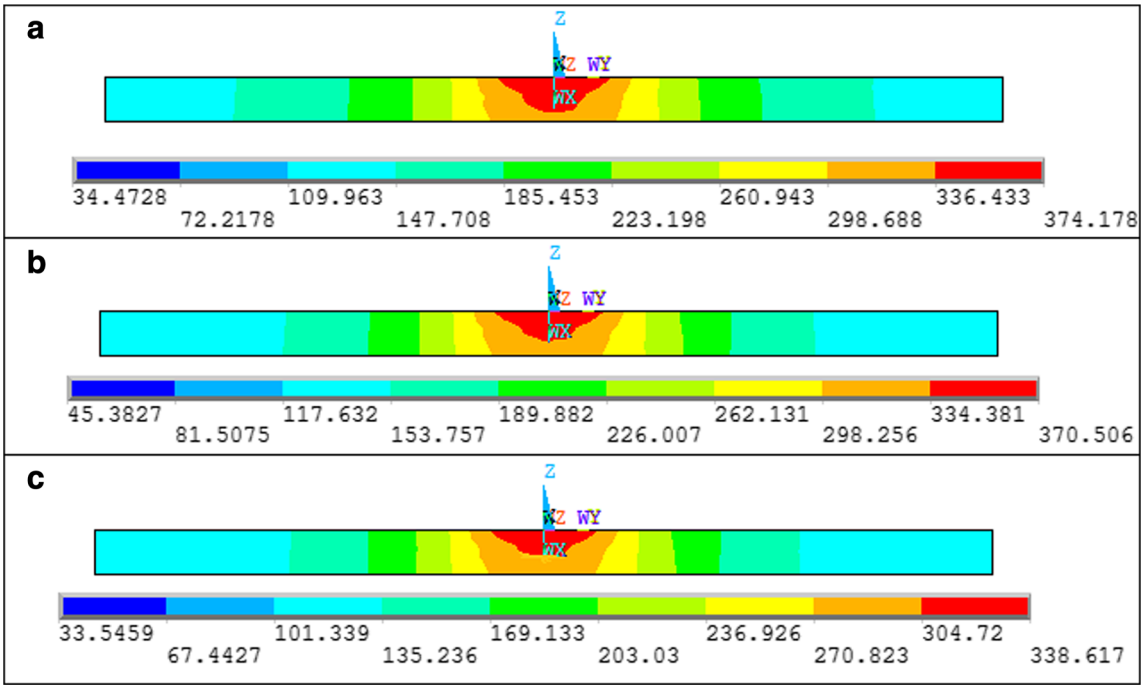

Fig. 11 Temperature distribution for immersed FSW along thickness direction for **a** asbestos, **b** mild steel, and **c** copper backing plate

Hardness distribution for air and immersed FSW carried out using various backing plates are shown in Figs. 13 and 14. Soft region has been formed at the NZ in all the joints welded using various backing plates which is typical characteristics of heat treatable aluminum alloys. Hardness profile shows "W" shape and lowest harness located in the NZ for all the cases. Hardness decreases from BM to TMAZ and a sudden rise is observed in NZ having hardness value ranging from 120 to 127 HV in air FSW. The same variation of hardness values for the immersed FSW joint is in the range of 129 to 139 HV. An increase in hardness at NZ both in air and immersed FSW shows strain hardening due to intense stirring by the rotating pin. It is observed from the hardness plot that the TMAZ is the weakest zone for all the FSW joints prepared using various backing plates for both air and immersed conditions. The welded joints show the drop in hardness at HAZ and TMAZ due to dissolution and growth of precipitates. It is evident from the Figs. 13 and 14 that the lowest hardness values have been obtained in FSW joints prepared using copper backing plate. This is due to higher cooling rates observed

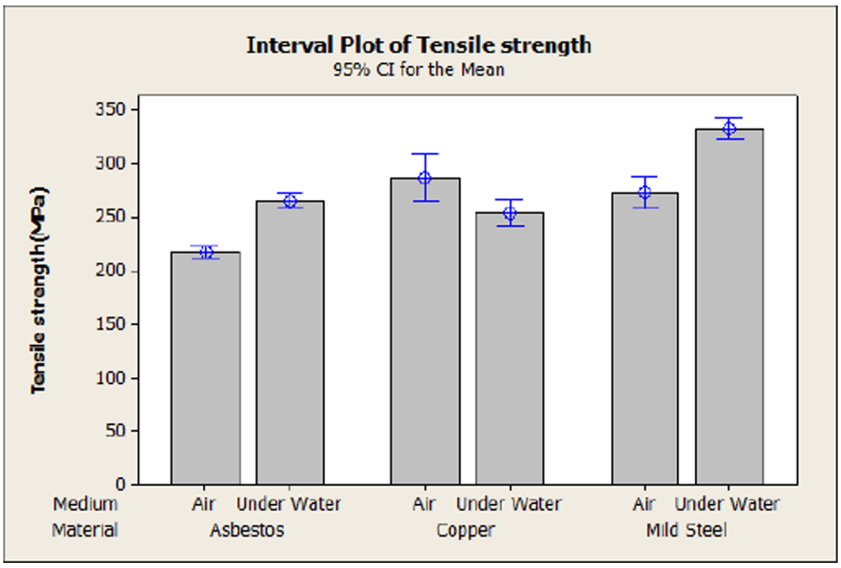

Fig. 12 Tensile strength of FSW joints for air and immersed FSW using various backing plates

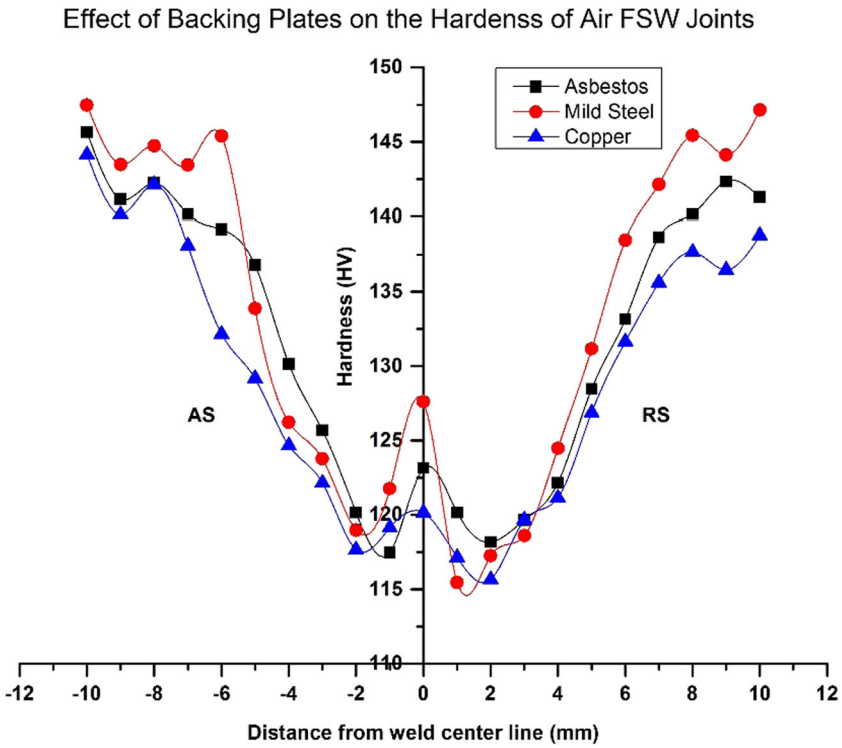

Fig. 13 Effect of backing plates on the hardness of air FSW joints

in copper backing plate which leads to improper material movement in the pin region. Similarly, lower hardness values obtained in the case of asbestos backing plate is also due to exposure of higher temperature in the weld region. Higher hardness values of joint have been observed while mild steel backing plate is used in both air and immersed FSW. This is due to a medium cooling rate while welding is in progress results in the defect-free pin region in the welded joint.

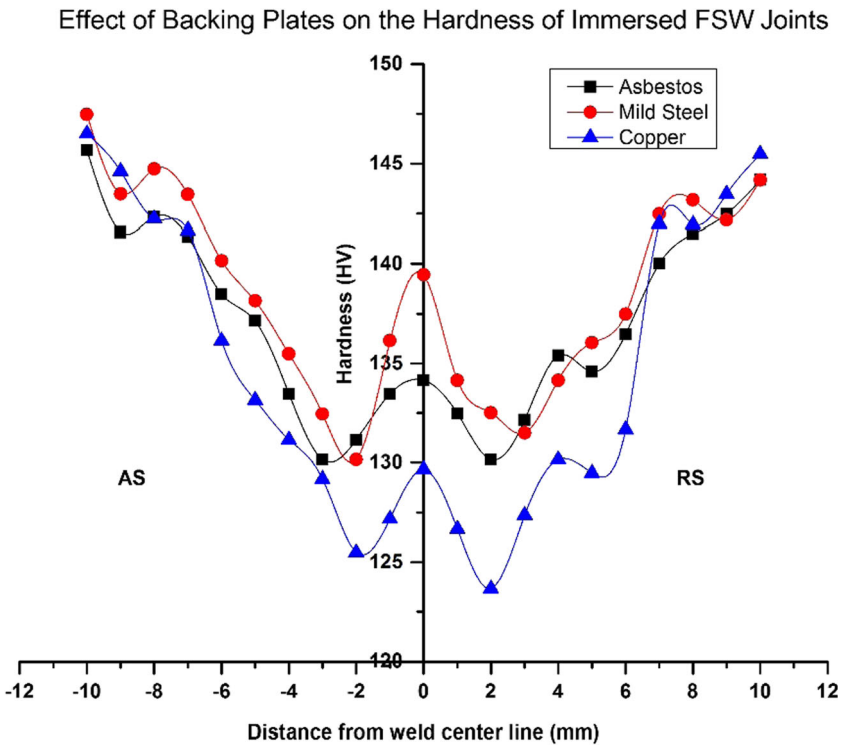

Fig. 14 Effect of backing plates on the hardness of immersed FSW joints

Lower dissolution of strengthening precipitates leads to higher hardness in immersed FSW compared to air FSW for all kinds of backing plates used for this study.

4 Conclusions

In present study, thermal numerical FE model for the air and immersed FSW has been developed using AA 2014-T6 as a workpiece material. The effects of the backing plates on the temperature profile and mechanical properties are also investigated.

1. Transient FE thermal simulation is carried out using commercially available FEA software ANSYS to predict the peak temperature during FSW of AA 2014-T6 aluminum alloy and the developed model is validated through experimental results. The simulation results obtained both for air and immersed FSW are in good agreement with those obtained experimentally. The developed thermal numerical model successfully predicts temperature in NZ within 3.5% error. The inclusion of heat generation due to plastic deformation in the mathematical model may improve the prediction of the temperature profile.
2. For immersed FSW, temperature rise and drop is sharp while for air FSW it is gradual. The immersed FSW exhibits a narrower high temperature distribution area compared to air FSW.
3. Studying the effect of various backing plates on microstructure, it is observed that diffusivity of backing plate affects the temperature of weld region. It is found that the plate having lower diffusivity has higher weld region temperature.
4. It is also observed that higher tensile strength and microhardness attained for the joints produced using mild steel backing plate in immersed FSW compared with other backing plates for same weld parameters. Maximum tensile strength obtained in an immersed FSW joint is around 17% higher than maximum strength obtained by air FSW joint. Thus, it is suggested to use immersed FSW for obtaining the higher tensile strength of the weld joint.

Funding The authors would like to appreciate financial supports from Science and Engineering Research Board (SERB) of Department of Science and Technology (DST), New Delhi, India, sanctioned through letter SR/S3/MERC/0108/2012.

Nomenclature α, Thermal diffusivity (m^2/s); t, Time (s); T, Current temperature (°C); q, Heat flux (W); u, Welding speed (m/s); k, Thermal conductivity (W/m K); q_{net}, Net heat flux in the control volume (W/m^2); T, Temperature of control volume (°C); T_o, Atmospheric temperature (°C); g, Gravitational acceleration (m/s^2); β, Coefficient of volume expansion (1/K); T_f, Bulk mean temperature (°C); t_s, Temperature of the surface (°C); t_a, Atmospheric temperature (°C); L, Characteristic length of the geometry (m); v, Kinematic viscosity of the fluid (m^2/s); k, Thermal conductivity (W/m K); R_{al}, Rayleigh number; N_u, Nusselt number; C_p, Specific heat (kJ/kg K); ρ, Density of fluid (kg/m^3); Q_p, Heat generated at pin interface (W); Q_s, Heat generated at shoulder interface (W); w, Angular velocity of the tool (rad/s); μ, Coefficient of friction; P, Uniform pressure (Pa); R_o, Tool shoulder radius (m); R_i, Tool pin radius (m)

References

1. Thomas WM, Nicholas ED, Needham JC, Murch MG, Templeshmith P, Dawes CJ (1991) G.B. patent application no. 9125978.8
2. Qin H, Zhang H, Wu H (2015) The evolution of precipitation and microstructure in friction stir welded2195-T8 Al–li alloy. Mater Sci Eng A 626:322–329
3. Kumar K, Kailas SV, Srivatsan TS (2011) The role of tool design in influencing the mechanism for the formation of friction stir welds in aluminium alloy 7020. Mater Manuf Process 26:915–921
4. Upadhyay P, Reynolds AP (2014) Effect of backing plate thermal property on friction stir welding of 25-mm-thick AA6061. Metall Mater Trans A 45:2091–2100
5. Hajinezhad M, Aziz A (2016) Numerical analysis of effect of coolant on the transient temperature in underwater friction stir welding of Al6061-T6. Int J Adv Manuf Technol 83(5):1241–1252
6. Liu HJ, Fujii H, Maeda M, Nogi K (2013) Tensile properties and fracture locations of friction-stir-welded joints of 2017-T351 aluminium alloy. J Mater Process Technol 142:692–696
7. Liang XP, Li HZ, Li Z, Hong T, Bing M, Liu SD, Liu Y (2012) Study on the microstructure in a friction stir welded 2519-T87 Al alloy. Mater Des 35:603–608
8. Fratini L, Buffa G, Shivpuri R (2009) In-process heat treatments to improve FS-welded butt joints. Int J Adv Manuf Technol 43:664–670
9. Fratini L, Buffa G, Shivpuri R (2010) Mechanical and metallurgical effects of in process cooling during friction stir welding of AA7075-T6 butt joints. Acta Mater 58:2056–2067
10. Liu HJ, Zhang HJ, Huang YX, Yu L (2010) Mechanical properties of underwater friction stir welded 2219 aluminum alloy. Trans Nonferrous Metals Soc China 20(8):1387–1391
11. Feng X, Liu H, Lippold JC (2013) Microstructure characterization of the stir zone of submerged friction stir processed aluminum alloy 2219. Mater Charact 82:97–102
12. Upadhyay P, Reynolds AP (2010) Effects of thermal boundary conditions in friction stir welded AA7050-T7 sheets. Mater Sci Eng A 527:1537–1543
13. Upadhyay P, Reynolds AP (2012) Effects of forge axis force and backing plate thermal diffusivity on FSW of AA6056. Mater Sci Eng A 558:394–402
14. Murshid I, Vikranth R, Kajal B (2015) Effect of backing plate material in friction stir butt and lap welding of 6063-T4 aluminium alloy. Int J Adv Manuf Technol 77:2181–2195
15. Zhang Z, Li W, Shen J, Chao YJ, Li J, Ma YE (2013) Effect of Backplate diffusivity on microstructure and mechanical properties of friction stir welded joints. Mater Des 50:551–557
16. Frigaard Ø, Grong Ø, Midling OT (2001) A process model for friction stir welding of age hardening aluminum alloys. Metall Mater Trans A 32(5):1189–1200
17. Colegrove PA, Shercliff HR (2005) 3-dimensional CFD modelling of flow round a threaded friction stir welding tool profile. J Mater Process Technol 169(2):320–327
18. Ulysse P (2002) Three dimensional modeling of friction stir welding. Int J Mach Tools Manuf 42(14):1549–1557

19. Chen CM, Kovacevic R (2003) Finite element modeling of friction stir welding – thermal and Thermomechnical analysis. Int J Mach Tools Manuf 43(3):1319–1326
20. Gök K, Aydin M (2013) Investigations of friction stir welding process using finite element method. Int J Adv Manuf Technol 68(1–4):775–780
21. Zhang XX, Xiao BL, Ma ZY (2011) A transient thermal model for friction stir weld. Part I: the model. Metall Mater Trans A 42(10): 3218–3228
22. Zhang HJ, Liu HJ, Yu L (2013) Thermal modeling of underwater friction stir welding of high strength aluminum alloy. Trans Nonferrous Metals Soc China 23(4):1114–1122
23. Ghetiya ND, Patel KM, Patel AB (2015) Prediction of temperature at weld line in air and immersed friction stir welding and its experimental validation. Int J Adv Manuf Technol 79:1239–1246
24. Bilgin MB, Gök K, Gök A (2015) Three-dimensional finite element model of friction drilling process in hot forming processes. Proc Inst Mech Eng Part E J Proc Mech Eng 231:548–554. https://doi.org/10.1177/0954408915614300
25. Neto DM, Neto P (2013) Numerical modeling of friction stir welding process: a literature review. Int J Adv Manuf Technol 65:115–126
26. Hahn DW, Ozisik MN (2012) Heat conductions, 3rd edn. Wiley, New York, USA
27. Prasanna P, Subba RB, Krishna Mohana RG (2010) Finite element modeling for maximum temperature in friction stir welding and its validation. Int J Adv Manuf Technol 51(9):925–933
28. Rajamanickam N, Balusamy V, Thyla PR, Vignesh GH (2009) Numerical simulation of thermal history and residual stresses in friction stir welding of aluminum 2014-T6. J Sci Ind Res 68:192–198
29. Holman JP (1997) Heat transfer. Mc Graw-Hill, Singapore
30. Chao YJ, Qi X (1998) Thermal and thermomechanical analysis of friction stir joining of AA6061-T6. J Mater Process Manuf Sci 7(2):215–233
31. Bastier A, Maitournam MH, Dang VK, Rioger F (2006) Steady state thermo mechanical modeling of friction stir welding. Sci Technol Weld Join 11(3):278–288
32. Schmidt H, Hattel J, Wert J (2004) An analytical model for the heat generation in friction stir welding. Model Simul Mater Sci Eng 12: 143–157